Electrical Conductivity, Chemistry, and Bonding Alternations under Graphene Oxide to Graphene Transition As Revealed by *In Situ* TEM

Zhi Xu,[†,‡] Yoshio Bando,[†] Lei Liu,[‡] Wenlong Wang,[‡] Xuedong Bai,[‡,*] and Dmitri Golberg[†,*]

[†]International Center for Materials Nanoarchitectonics (MANA), National Institute for Materials Science (NIMS), 1-1 Namiki, Tsukuba, Ibaraki 305-0044, Japan, and
[‡]Beijing National Laboratory for Condensed Matter Physics, Institute of Physics, Chinese Academy of Sciences, Beijing 100190, China

ABSTRACT A suspended graphene oxide device is fabricated and investigated using a transmission electron microscope (TEM) scanning tunneling microscope (STM) setup. A detailed study of step-by-step reduction of an individual graphene oxide sheet under current flow and Joule heating in tandem with conductivity measurements, atomic structure imaging, chemical composition, and bonding alternations tracing is performed. As monitored by electron energy loss spectroscopy, the oxygen content is tuned from that peculiar to a pristine graphene oxide (*i.e.*, 23.8 at %) to oxygen-free pure graphene. Six orders of magnitude conductance rise is observed during this process with the final conductivity reaching 1.5×10^5 S/m. Quantification of plasma energy losses of the starting graphene oxide shows that ~40% of the oxygen atoms are in the form of epoxy, and ~60% oxygen atoms are in the form of hydroxyl. The total portion of sp^3 bonds in pristine graphene oxide is estimated to be ~45%. The epoxy groups show a larger influence on the conductivity of graphene oxide than hydroxyl ones. Through analyzing consecutive plasma-loss energy spectra under gradual graphene oxide to graphene transformation, it is found that the oxygen atoms in epoxy groups decompose prior to those in hydroxyl groups.

KEYWORDS: graphene · graphene oxide · electron energy loss spectroscopy (EELS) · *in situ* TEM

Graphene is a one-atom-thick layer of graphite with two linear bands crossing at the Dirac point. Due to such unique electronic structure, the prospects of graphene-based nanoelectronics have stimulated extensive research activities.[1−9] Although single layers of graphene have been prepared by mechanical cleavage,[1] calcinations of SiC,[10,11] and CVD growth on transition metals,[12,13] the central challenge of graphene implementation is its mass production. A promising solution to this problem comprises chemical conversion of readily accessible monolayers of graphene oxide to graphene.[14−16] Graphene oxide has its own advantages. First, the exfoliation of graphite oxide is efficient and results in high yields of single-layered graphene oxide flakes.[16] Second, good solubility of graphene oxide in water and other solvents allows it to be uniformly deposited onto a wide range of substrates in the form of thin films or networks which are valuable for nanoelectronic devices.[17,18] Third, graphene oxide is an insulator, but a controlled oxidation provides a way to tune its electronic properties, optical transparency, and mechanical characteristics.[19−21] Such features hold significant promise for novel sensors, optoelectronic devices, and smart composites.

To date, it has generally been accepted that a sheet of graphene oxide forms over a range of O:C compositions with the oxygen bound to carbon both at the top and at the bottom of a honeycomb lattice in the form of hydroxyl and epoxy functional groups, whereas the sheet edges are mostly decorated by carbonyl and carboxyl groups. Although tuning the conductivity of a graphene oxide sheet by thermal annealing reduction has successfully been demonstrated,[20,23−26] the detailed nanostructure evolution and chemical composition changes during this process have not been elucidated as yet. It worth noting that before graphene oxide can be used for many technological applications it is important to understand its detailed chemical reduction kinetics.

In this work, a specially designed graphene oxide device was fabricated and investigated in a transmission electron microscope (TEM)-based setup which allowed us to perform in-tandem conductance measurements and real-time TEM observations at a high spatial resolution. The graphene oxide sheet was reduced step-by-step by a gradual increase of temperature under its Joule heating. The atomic structure changes were monitored by high-resolution TEM.

* Address correspondence to xdbai@aphy.iphy.ac.cn, golberg.dmitri@nims.go.jp.

Received for review November 24, 2010 and accepted May 10, 2011.

Published online May 10, 2011
10.1021/nn103200t

The sheet's chemical composition and bonding states were characterized by electron energy loss spectroscopy (EELS). The graphene oxide sheet was finally reduced to an oxygen-free pure graphene; its resistance dropped from >1 GΩ to 10 kΩ (corresponding to a conductivity of 1.5×10^5 S/m). Consecutive deoxidation stages were systematically studied.

RESULTS AND DISCUSSION

A suspended graphene oxide sheet was placed in a TEM, and an electrical contact was made to it. The geometry of the design is shown in Figure 1a. A low-magnification TEM image of the cantilevered graphene oxide device is shown in Figure 1b. A high-resolution image and the corresponding fast Fourier transform (FFT) pattern show that the graphene oxide sheet has an amorphous-like structure. Using a dipping method (see details in the Experimental Method), we typically produced sheets made of 3−5 layers of graphene oxide, rather than of a single layer (see the bottom inset in Figure 1d). Since graphene oxidation is random throughout a single graphene layer, C−O bonds break the symmetry of the original honeycomb carbon lattice. Therefore, when several single graphene oxide layers are randomly stacked to form a sheet, the lattice fringes peculiar to a pure graphene cannot be resolved. At the beginning, the graphene oxide sheet was highly electrically resistant with a resistance >1 GΩ. We gradually increased the maximum bias (and thus the Joule heating temperature), and the consecutive current measurement cycles were performed in series. The resistance of the sheet decreased after each cycle. The serial *I*−*V* curves are shown in Figure 2a,b using a linear scale and in Figure 2c using a logarithmic scale. From the logarithmic plot, one can clearly see that a passing current increases 6 orders of magnitude, and so does the conductance.

After each *I*−*V* measurement, we performed detailed EELS analysis of the sheet. As seen from the core loss spectra, both carbon and oxygen peaks are visible. Quantification of the spectrum 1 (Figure 3a) gives a 23.84 at % oxygen content in the pristine graphene oxide. The oxygen content decreases after each *I*−*V* measurement until pure graphene is finally obtained (spectrum 7, Figure 3a). The corresponding *I*−*V* curve (Figure 2b, plot 7) displays a linear character attributable to the Ohmic contacts between the metal electrodes and the pure graphene. In the previous study, when graphene oxide was heated to 1100 °C, there was still about 8 at % oxygen left.[23,24] In our study, during the final cycle, a current exceeded 2 mA under a 18 V bias. In the previous report on Joule heating of a carbon nanotube[27] and a pure graphene,[28] Huang *et al.* used the thermal-induced lattice expansion of nanotube walls (from 0.34 to 0.4 nm) to estimate the temperature. Here, the electrical circuit and current density (1.2×10^7 A/cm^2) are close to those applied in the Huang's experiments, and thus we assume that the temperature may also exceed 2000 °C during the final Joule heating cycle, as was verified in the former work.

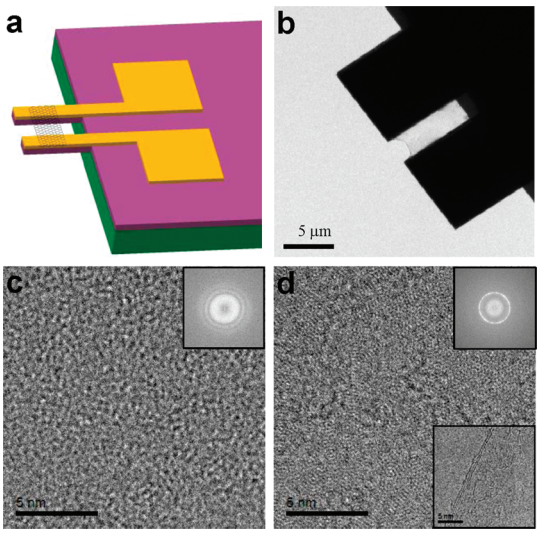

Figure 1. (a) Schematic drawing of a suspended free-standing graphene oxide device mounted into the high-resolution transmission electron microscope. Silicon nitride cantilevers are used to support gold electrodes on which the graphene oxide sheet is deposited. (b) Low-magnification TEM image of the graphene oxide device. Graphene oxide sheet can be seen in the space between two cantilever electrodes. (c) High-resolution TEM image of the pristine graphene oxide sheet. Inset: fast Fourier transform image showing that the pristine graphene oxide sheet is amorphous. (d) High-resolution TEM image of the graphene oxide sheet after its complete reduction. Top inset: fast Fourier transform image showing {10−10} diffraction ring, which indicates the sample graphitization. Bottom inset: high-resolution TEM image of the sheet edge after reduction; 3−5 layers are seen.

Each carbon K-edge EEL spectrum consists of a peak at around 284 eV due to excitations from the 1s level to empty π^* states of the sp^2-bonded atoms, followed by a step at around 289 eV due to a transition from the 1s level to empty σ^* states at both sp^2- and sp^3-bonded atoms. During the regarded Joule heating-induced chemical reduction process, the fine structure of the C K-edge also displays a notable change. At the beginning (no. 1 spectrum, Figure 3a,b), the π^* peak is hardly seen. With the oxygen content decreasing, this peak becomes more and more intense. The σ^* peak also becomes sharper when the pure graphene is obtained. These changes demonstrate the chemical bonding alternations during the Joule heating cycles. As indicated in Figure 1c, the pristine graphene oxide exhibits an amorphous-like structure. Oxygen forms sp^3 C−O bonds with carbon, and the sp^2 bonding fraction is relatively low. When oxygen is consumed, sp^2-bonded C atoms eventually dominate, and the sample becomes more and more graphitized. Sharpening of EELS peaks indicates that crystallization improves after *in situ* TEM Joule heating/annealing. This result coincides with the HRTEM images shown in Figure 1d.

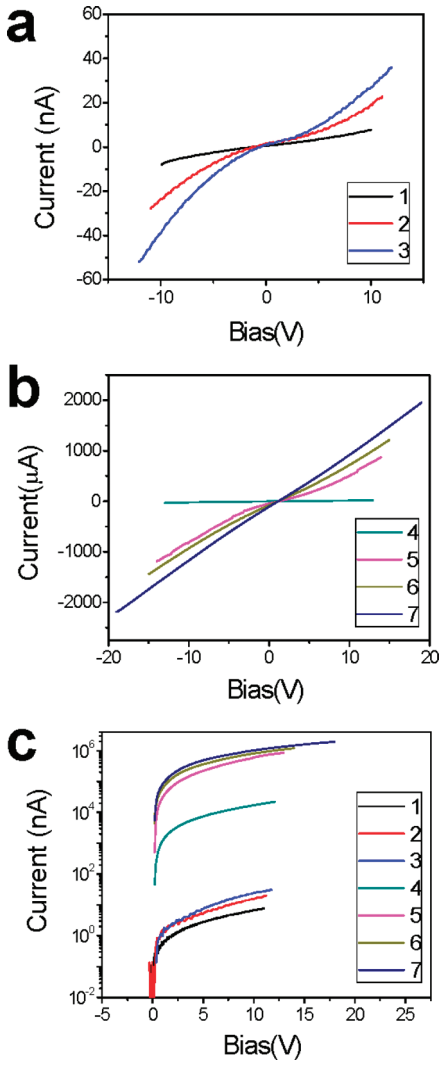

Figure 2. (a) First three *I*−*V* curves at the initial stage of the graphene oxide chemical reduction. (b) Latter four *I*−*V* curves at the final stage. Curves gradually change their character from nonlinear to linear. No oxygen is detected in the EEL spectrum during the measurement #7. (c) In order to evaluate the change in current, the *I*−*V* curves from #1 to #7 are plotted in the logarithmic scale. From #1 to #7, 6 orders of magnitude increase in current is apparent.

The sp^2/sp^3 atomic ratio can also be deduced from the plasmon energy loss range of the EEL spectra, which is derived from the corresponding valence states' alternations. From the low loss EEL spectra recorded along with the *I*−*V* measurement cycles (*e.g.*, Joule heating cycles), one can see a notable red shift of the plasmon energy when the oxygen content decreases. When this observation is combined with the elemental quantification analysis using Figure 3a, the plasmon energies as a function of the oxygen content are summarized in Figure 3d. The plasmon energy of the pristine graphene oxide is ~24.5 eV; this value for the oxygen-free pure graphene sheet becomes ~22.7 eV. Previously, it has been found that π^* and $\pi^* + \sigma^*$ plasmon modes in a free-standing graphene sheet are substantially red-shifted compared to their values in graphite. The experimentally recorded $\pi^* + \sigma^*$ plasmon energies for a single layer and a five layer graphene are 14.6 and 18 eV, respectively.[29,30] When the thickness of a graphene flake exceeds 10 atomic layers, its plasmon energy approaches that of bulk graphite (*i.e.*, 26 eV). Thus 22.7 eV plasmon energy for a 3−5 layer graphene sheet in our experiments looks reasonable. The low-energy plasma excitations of the π^* electrons in the graphene oxide sheet sample take place at the energy of ~6 eV, which is lower than that in graphite (*i.e.*, ~7 eV) but higher than that in a single graphene oxide sheet (*i.e.*, ~5 eV) and in a single-layer graphene (*i.e.*, 4.7 eV).[29−31] The positions of these π^* electron plasma excitations do not show an obvious change when the graphene oxide sheets are reduced to graphene.

The plasmon energy of a pristine graphene oxide sheet, 24.5 eV, is higher than that in graphene because of the sp^3 hybridization induced by the oxygen-containing groups. On the basis of the previous studies and the free electron model, the plasmon energy decreases almost linearly with sp^3 fraction decreasing.[32,33] The plasmon energy of an amorphous carbon sample, which has ~45% fraction of sp^3 bonds, is around 24 eV.[31] It is reasonable to suggest that in our pristine graphene oxide sample the actual amount of carbon sp^3 bonds is also around 45%. Connecting the plasmon energy with the oxygen content (shown in Figure 3d), we conclude that this energy change takes place in two stages: a decreasing rate is 2 times faster at the starting than in final stages. Since plasmon energy is linearly related with the sp^3 bond fraction, if a same amount of oxygen is released from graphene oxide, 2 times more sp^3 bonds are broken during the starting than during the final stages. The sp^3 to sp^2 transition mainly takes place in the basal plane, where the epoxy and hydroxyl groups coexist. Considering that in the epoxy group one O atom bonds to two C atoms, whereas in the hydroxyl one O atom bonds to only one C atom (see atomic models in Figure 3d), it is concluded that at the beginning mainly epoxy groups decompose, and latter hydroxyl groups start to decompose. *Ab initio* calculation demonstrates that the formation energy of hydroxyl is more than 2 times larger than that of the epoxy.[21] By contrast, using molecular dynamic simulations of graphene oxide thermal annealing, the epoxy groups were found to be relatively more stable than the hydroxyl ones.[22] This discrepancy clearly indicates that the atomic structure evolution of graphene oxide during thermal annealing is still an open question which requires further investigations. The present analysis also suggests that the ratio of hydroxyl groups to epoxy groups in a graphene oxide is 14.5%: (23.8−14.5%) ≈ 3:2. We have to point out that graphene oxide is not stoichiometric and is highly hygroscopic, and hence its composition can vary with the synthesis methods and environments.[16,23] We additionally carried out X-ray photoelectron spectroscopy (XPS) analysis of the starting graphene oxide materials,

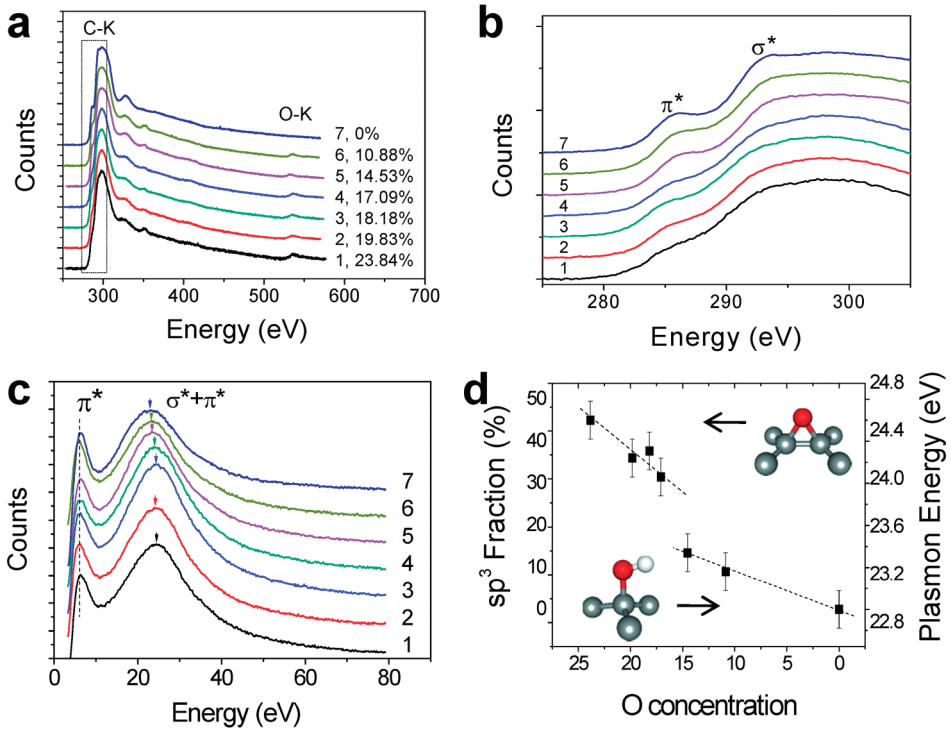

Figure 3. (a) EEL core loss K-edges of C (284 eV) and O (532 eV) at different graphene oxide chemical reduction stages. Quantification of the C and O K-edges is carried out to calculate the atomic ratio of the species; this is shown on the right-hand side of each spectrum. (b) Enlarged view of the C K-edge. The evolution of π^* peak is evident. (c) Plasmon energy spectra at different reduction stages. The π^* peak does not show an obvious change, whereas the $\pi^* + \sigma^*$ peak red shifts. (d) Plasmon energy as a function of the O content. Generally, plasmon energy decreases with decreasing O content; the decreasing rate at the initial stage is twice as fast compared to the final stage. The dashed line is drawn as a guide to the eye. Since the plasmon energy is linearly proportional to the sp^3 bond fraction, the sp^3 fraction label is added on the left-hand side of *y* axis. Atomic models of epoxy and hydroxyl complexes are shown. Carbon, gray; oxygen, red; hydrogen, white.

which we used for the present *in situ* TEM experiments. The ratio of hydroxyl groups to epoxy groups deduced from the C 1s peak on the XPS spectrum was about 1.4, which is consistent with the EELS analysis data (see Supporting Information).

Now, we are able to link the conductance of the graphene oxide sheet to its oxygen content, as shown in Figure 4. The conductance is calculated from the linear section of each *I*−*V* curve in a high-voltage regime. At the initial stage, the conductance increases rapidly under release of oxygen, whereas at the final stage, the increase rate becomes comparatively slow. Comparing the conductance change (Figure 4) with the plasmon energy shift (Figure 3d), one can see that when the plasmon energies red shift rapidly (corresponding to the epoxy decomposition) the conductance also drastically increases, whereas when the plasmon energy change becomes slow, the conductance also does not notably change. For the epoxy group, one O atom bonds to two C atoms, and such groups mainly exist on graphitic basal planes. When O atoms from the epoxy groups are released, the graphene oxide lattice transforms to a perfect graphene structure and its conductance dramatically increases. *Ab initio* calculations have also shown that an epoxy dopant can more easily introduce a band gap in graphene than a hydroxyl one.[21]

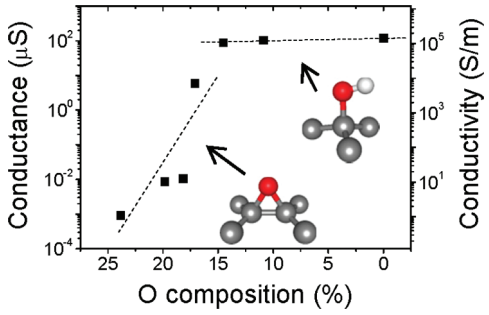

Figure 4. Conductance and conductivity of a sheet sample as a function of O content. At the initial stage, conductance increases very rapidly, while at the final stage, the increase becomes slow. Atomic models of epoxy and hydroxyl complexes are added for clarity. Carbon, gray; oxygen, red; hydrogen, white.

CONCLUSION

In summary, different deoxidation stages of a graphene oxide sheet, from as-prepared material to oxygen-free pure graphene, were studied under controllable step-by-step Joule heating inside a high-resolution transmission electron microscope. The process was monitored and analyzed using EELS combined with in-tandem conductance measurements and high-resolution imaging. An oxygen content decrease, as determined by quantification of the core loss

EEL spectra, resulted in a 6 orders of magnitude increase in sheet conductance. During the sheet reduction, the transformation of sp^3-hybridized states to sp^2-hybridized ones was verified under plasmon energy red shift observations. Quantitative analysis of the plasmon peak fine structure showed that the epoxy O groups of the graphene oxide had decomposed prior to the hydroxyl ones. As a result, the sheet conductivity rapidly increased at the beginning of graphene oxide to graphene phase transformation but slowed toward the end. Since, until now, no solid evidence or feasible methods have been demonstrated to show that during the synthesis graphene can selectively be oxidized by one of the regarded oxygen-containing groups, the present elucidation of the effect of different oxygen groups on graphene oxide conductivity and its changes during transition to graphene is envisaged to be valuable for these material integrations into various technologies.

EXPERIMENTAL METHOD

A graphene oxide sample was prepared by the modified Hummers method. A suspension of graphene oxide flakes in distilled water was obtained[18] (see details in Supporting Information). In order to perform the electrical measurements inside a TEM, we designed a suspended graphene oxide device in which cantilever electrodes were used to support a graphene oxide sheet and to make electrical contact to it. The geometry of the design is shown in Figure 1a. A silicon nitride film was etched into two cantilevers; on top of these, gold electrodes were fabricated (see details in Supporting Information). When the blank device was made, the cantilever electrodes were dipped into a graphene oxide suspension for a short period of time under micropositioning in an optical microscope. When a graphene oxide flake was seen to be successfully placed between the cantilevers, the device was finally completed and mounted inside a "Nanofactory Instruments" multiprobe STM-TEM holder for high-resolution imaging and in-parallel electrical measurements inside a field-emission HRTEM (JEOL 3100FEF) equipped with an in-column Omega filter and, thus, with EELS capabilities. Then the *I*−*V* measurements were performed on this free-standing graphene oxide device. Due to a Joule heating effect when a current flows over the graphene oxide sheet, it was heated to a certain temperature (up to 2000 °C in the final cycle). When each *I*−*V* cycle was completed, HRTEM images were recorded and EEL spectra were acquired. Then, we used a larger bias voltage (compared to the previous *I*−*V* cycle) to perform a new *I*−*V* measurement. That means that in each consecutive cycle the graphene oxide sheet was heated to a higher temperature than during the previous *I*−*V* cycle. In this way, the same graphene oxide sheet was thermally reduced step-by-step under in-steps increasing temperature during each consecutive measurement. A gradual decrease of the oxygen peak during EELS was documented, and finally, an oxygen-free material—a pure graphene sheet—was obtained.

Acknowledgment. This work was supported by the International Center for Materials Nanoarchitectonics (MANA) of the National Institute for Materials Science (NIMS), Japan, and the NSF (Nos. 10874218, 50725209, and 11004230) and MOST (Nos. 2007CB936203 and 2007AA03Z353) of China.

Supporting Information Available: Additional experimental details. This material is available free of charge *via* the Internet at http://pubs.acs.org.

REFERENCES AND NOTES

1. Geim, A. K.; Novoselov, K. S. The Rise of Graphene. *Nat. Mater.* **2007**, *6*, 183–191.
2. Novoselov, K. S.; Geim, A. K.; Morozov, S. V.; Jiang, D.; Zhang, Y.; Dubonos, S. V.; Grigorieva, I. V.; Firsov, A. A. Electric Field Effect in Atomically Thin Carbon Films. *Science* **2004**, *306*, 666–669.
3. Ohta, T.; Bostwick, A.; Seyller, T.; Horn, K.; Rotenberg, E. Controlling the Electronic Structure of Bilayer Graphene. *Science* **2006**, *313*, 951–954.
4. Han, M. Y.; Ozyilmaz, B.; Zhang, Y.; Kim, P. Energy Band-Gap Engineering of Graphene Nanoribbons. *Phys. Rev. Lett.* **2007**, *98*, 206805.
5. Giovannetti, G.; Khomyakov, P.; Brocks, G.; Kelly, P. J.; Brink, J. Substrate-Induced Band Gap in Graphene on Hexagonal Boron Nitride: *Ab Initio* Density Functional Calculations. *Phys. Rev. B* **2007**, *76*, 073103.
6. Li, X.; Wang, X.; Zhang, L.; Lee, S.; Dai, H. Chemically Derived, Ultrasmooth Graphene Nanoribbon Semiconductors. *Science* **2008**, *319*, 1229–1232.
7. Wu, X.; Sprinkle, M.; Li, Xu; Ming, F.; Berger, C.; de Heer, W. A. Epitaxial-Graphene/Graphene-Oxide Junction: An Essential Step towards Epitaxial Graphene Electronics. *Phys. Rev. Lett.* **2008**, *101*, 026801.
8. Eda, G.; Chhowalla, M. Chemically Derived Graphene Oxide: Towards Large-Area Thin-Film Electronics and Optoelectronics. *Adv. Mater.* **2010**, *22*, 2392–2415.
9. Elias, D. C.; Nair, R. R.; Mohiuddin, T. M. G.; Morozov, S. V.; Blake, P.; Halsall, M. P.; Ferrari, A. C.; Boukhvalov, D. W.; Katsnelson, M. I.; Geim, A. K.; *et al.* Control of Graphene's Properties by Reversible Hydrogenation: Evidence for Graphene. *Science* **2009**, *323*, 610–613.
10. Berger, C.; Song, Z.; Li, X.; Wu, X.; Brown, N.; Naud, C.; Mayou, D.; Li, T.; Hass, J.; Marchenkov, A. N.; *et al.* Electronic Confinement and Coherence in Patterned Epitaxial Graphene. *Science* **2006**, *312*, 1191–1196.
11. Zhou, S. Y.; Gweo, G. H.; Fedorov, A. V.; First, P. N.; de Heer, W. A.; Lee, D. H.; Guinea, F.; Neto, A. H. C.; Lanzara, A. Substrate-Induced Bandgap Opening in Epitaxial Graphene. *Nat. Mater.* **2007**, *6*, 770–775.
12. Marchini, S.; Gunther, S.; Wintterlin, J. Scanning Tunneling Microscopy of Graphene on Ru(0001). *Phys. Rev. B* **2007**, *76*, 075429.
13. Pan, Y.; Zhang, H. G.; Shi, D. X.; Sun, J. T.; Du, S. X.; Liu, F.; Gao, H.-J. Highly Ordered, Millimeter-Scale, Continuous, Single-Crystalline Graphene Monolayer Formed on Ru (0001). *Adv. Mater.* **2009**, *21*, 2777–2780.
14. Stankovich, S.; Piner, R. D.; Chen, X. Q.; Wu, N. Q.; Nguyen, S. T.; Ruoff, R. S. Stable Aqueous Dispersions of Graphitic Nanoplatelets *via* the Reduction of Exfoliated Graphite Oxide in the Presence of Poly(sodium 4-styrenesulfonate). *J. Mater. Chem.* **2006**, *16*, 155–158.
15. Gomez-Navarro, C.; Weitz, R. T.; Bittner, A. M.; Scolari, M.; Mews, A.; Burghard, M.; Kern, K. Electronic Transport Properties of Individual Chemically Reduced Graphene Oxide Sheets. *Nano Lett.* **2007**, *7*, 3499–3503.
16. Stankovich, S.; Dikin, D. A.; Piner, R. D.; Kohlhaas, K. A.; Kleinhammes, A.; Jia, Y.; Wu, Y.; Nguyen, S. T.; Ruoff, R. S. Synthesis of Graphene-Based Nanosheets *via* Chemical Reduction of Exfoliated Graphite Oxide. *Carbon* **2007**, *45*, 1558–1565.
17. Eda, G.; Fanchini, G.; Chhowalla, M. Large-Area Ultrathin Films of Reduced Graphene Oxide as a Transparent and Flexible Electronic Material. *Nat. Nanotechnol.* **2008**, *3*, 270–274.
18. Fu, W. Y.; Liu, L.; Wang, W. L.; Wu, M. H.; Xu, Z.; Bai, X. D.; Wang, E. G. Carbon Nanotube Transistors with Graphene Oxide Films as Gate Dielectrics. *Sci. China Ser. G* **2010**, *53*, 828–833.

19. Eda, G.; Lin, Y.-Y; Mattevi, C.; Yamaguchi, H.; Chen, H.-A.; Chen, I.-S.; Chen, C.-W.; Chhowalla, M. Blue Photoluminescence from Chemically Derived Graphene Oxide. *Adv. Mater.* **2010**, *22*, 505–509.
20. Jung, I.; Dikin, D. A.; Piner, R. D.; Ruoff, R. S. Tunable Electrical Conductivity of Individual Graphene Oxide Sheets Reduced at "Low" Temperatures. *Nano Lett.* **2008**, *8*, 4283–4287.
21. Yan, J.-A.; Xian, L.; Chou, M. Y. Structural and Electronic Properties of Oxidized Graphene. *Phys. Rev. Lett.* **2009**, *103*, 086802.
22. Bagri, A.; Mattevi, C.; Acik, M.; Chabal, Y. J.; Chhowalla, M.; Shenoy, V. B. Structural Evolution during the Reduction of Chemically Derived Graphene Oxide. *Nat. Chem.* **2010**, *2*, 581–587.
23. Mattevi, C.; Eda, G.; Agnoli, S.; Miller, S.; Mkhoyan, K. A.; Celik, O.; Mastrogiovanni, D.; Granozzi, G.; Garfunkel, E.; Chhowalla, M. Evolution of Electrical Chemical and Structural Properties of Transparent and Conducting Chemically Derived Graphene Thin Films. *Adv. Funct. Mater.* **2009**, *19*, 2577–2583.
24. McAllister, M. J.; Li, J.-L.; Adamson, D. H.; Schniepp, H. C.; Abdala, A. A.; Liu, J.; Herrera-Alonso, M.; Milius, D. L.; Car, R.; Prud'homme, R. K.; *et al.* Single Sheet Functionalized Graphene by Oxidation and Thermal Expansion of Graphite. *Chem. Mater.* **2007**, *19*, 4396–4404.
25. Eda, G.; Mattevi, C.; Yamaguchi, H.; Kim, H.; Chhowalla, M. Insulator to Semimetal Transition in Graphene Oxide. *J. Phys. Chem. C* **2009**, *113*, 15768–15771.
26. Jung, I.; Field, D. A.; Clark, N. J.; Zhu, Y.; Yang, D.; Piner, R. D.; Stankovich, S.; Dikin, D. A.; Geisler, H.; Ventrice, C. A., Jr.; *et al.* Reduction Kinetics of Graphene Oxide Determined by Electrical Transport Measurements and Temperature Programmed Desorption. *J. Phys. Chem. C* **2009**, *113*, 18480–18486.
27. Huang, J. Y.; Chen, S.; Jo, S. H.; Wang, Z.; Han, D. X.; Chen, G.; Dresselhaus, M. S.; Ren, Z. F. Atomic-Scale Imaging of Wall-by-Wall Breakdown and Concurrent Transport Measurements in Multiwall Carbon Nanotubes. *Phys. Rev. Lett.* **2005**, *94*, 236802.
28. Huang, J. Y.; Ding, F.; Yakobson, B. I.; Lu, P.; Qi, L.; Li, J. *In Situ* Observation of Graphene Sublimation and Multi-layer Edge Reconstructions. *Proc. Natl. Acad. Sci. U.S.A.* **2009**, *106*, 10103–10108.
29. Eberlein, T.; Bangert, U.; Nair, R. R.; Jones, R.; Gass, M.; Bleloch, A. L.; Novoselov, K. S.; Geim, A.; Briddon, P. R. Plasmon Spectroscopy of Free-Standing Graphene Films. *Phys. Rev. B* **2008**, *77*, 233406.
30. Gass, M. H.; Bangert, U.; Bleloch, A. L.; Wang, P.; Nair, R. R.; Geim, A. K. Free-Standing Graphene at Atomic Resolution. *Nat. Nanotechnol.* **2008**, *3*, 676–681.
31. Mkhoyan, K. A.; Contryman, A. W.; Silcox, J.; Stewart, D. A.; Eda, G.; Mattevi, C.; Miller, S.; Chhowalla, M. Atomic and Electronic Structure of Graphene-Oxide. *Nano Lett.* **2009**, *9*, 1058–1063.
32. Fallon, P. J.; Veerasamy, V. S.; Davis, C. A.; Robertson, J.; Amaratunga, G. A. J.; Milne, W. I.; Koskinen, J. Properties of Filtered-Ion-Beam-Deposited Diamondlike Carbon as a Function of Ion Energy. *Phys. Rev. B* **1993**, *48*, 4777–4782.
33. Yuan, J.; Brown, L. M. Investigation of Atomic Structure of Diamond-like Amorphous Carbon by Electron Energy Loss Spectroscopy. *Micron* **2001**, *31*, 515–525.